The ZM Grid: An Alternative to the Z Grid

TODD D. RINGLER AND DAVID A. RANDALL

Department of Atmospheric Science, Colorado State University, Fort Collins, Colorado

(Manuscript received 4 June 2001, in final form 30 November 2001)

ABSTRACT

Shallow-water equations discretized on a perfect hexagonal grid are analyzed using both a momentum formulation and a vorticity-divergence formulation. The vorticity-divergence formulation uses the unstaggered Z grid that places mass, vorticity, and divergence at the centers of the hexagons. The momentum formulation uses the staggered ZM grid that places mass at the centers of the hexagons and velocity at the corners of the hexagons. It is found that the Z grid and the ZM grid are identical in their simulation of the physical modes relevant to geostrophic adjustment. Consistent with the continuous system, the simulated inertia–gravity wave phase speeds increase monotonically with increasing total wavenumber and, thus, all waves have nonzero group velocities.

Since a grid of hexagons has twice as many corners as it has centers, the ZM grid has twice as many velocity points as it has mass points. As a result, the ZM-grid velocity field is discretized at a higher resolution than the mass field and, therefore, resolves a larger region of wavenumber space than the mass field. We solve the $\nabla^2 f = \lambda f$ eigenvalue problem with periodic boundary conditions on both the Z grid and ZM grid to determine the modes that can exist on each grid. The mismatch between mass and momentum leads to computational modes in the velocity field. Two techniques that can be used to control these computational modes are discussed. One technique is to use a dissipation operator that captures or ''sees'' the smallest-scale variations in the velocity field. The other technique is to invert elliptic equations in order to filter the high wavenumber part of the momentum field.

Results presented here lead to the conclusion that the ZM grid is an attractive alternative to the Z grid, and might be particularly useful for ocean modeling.

1. Introduction

The Z grid was introduced by Randall (1994) as an attractive alternative to the conventional A–E-grid staggering systems (Arakawa and Lamb 1977) commonly used in finite-difference models with quadrilateral grid cells. The Z grid uses the vorticity-divergence form of the shallow-water equations without staggering (Fig. 1a). Randall (1994) found that the Z grid simulates the geostrophic adjustment process better than any of the A–E-grid staggering systems.

When using the vorticity-divergence form of the nonlinear shallow-water equations, it is necessary to invert elliptic equations after every time step in order to obtain the velocity field. Heikes and Randall (1995a,b) implemented multigrid techniques to invert these equations efficiently when the domains extend over the entire sphere. These domains, which are singly connected and periodic, are particularly accommodating to the use of multigrid methods. In contrast, the domains of ocean models are generally neither singly connected nor periodic. The existence of islands and the lateral boundary conditions pose significant obstacles to inverting the elliptic equations in a computationally efficient manner. This suggests that the Z grid may be impractical for use in ocean models.

In recent work that focuses on the nonlinear aspects of the shallow-water equations on a spherical geodesic grid, Ringler and Randall (2002, hereafter RR) identify a discrete momentum equation consistent with the Z-grid vorticity-divergence equations. This discrete momentum formulation, termed the ZM grid, places scalar quantities, such as mass, at grid cell centers, and vectors, such as velocity, at all grid cell corners (See Fig. 1b).

The Z and ZM grids are not the only staggerings possible on the hexagonal grid. Mesinger (2000) discusses the hexagonal grid analogs to the A, B, C, and D grids that are referred to as the HA, HB, HC, and HD grids, respectively. The well-known deficiencies of the A and D grids are also present on the HA and HD grids [see Randall (1994) for discussion of the A and D grids]. The HB grid uses a full velocity vector at *every other* corner in order to obtain a one-to-one correspondence between the mass points and the velocity points. The HC grid predicts only the normal component of the velocity field at the midpoint of each cell wall. Nickovic and Mesinger (as discussed in Purser 1998) show that both the HB and HC grid generate nonsta-

Corresponding author address: Todd Ringler, Department of Atmospheric Science, Colorado State University, Fort Collins, CO 80523-1371.
E-mail: todd@atmos.colostate.edu

© 2002 American Meteorological Society

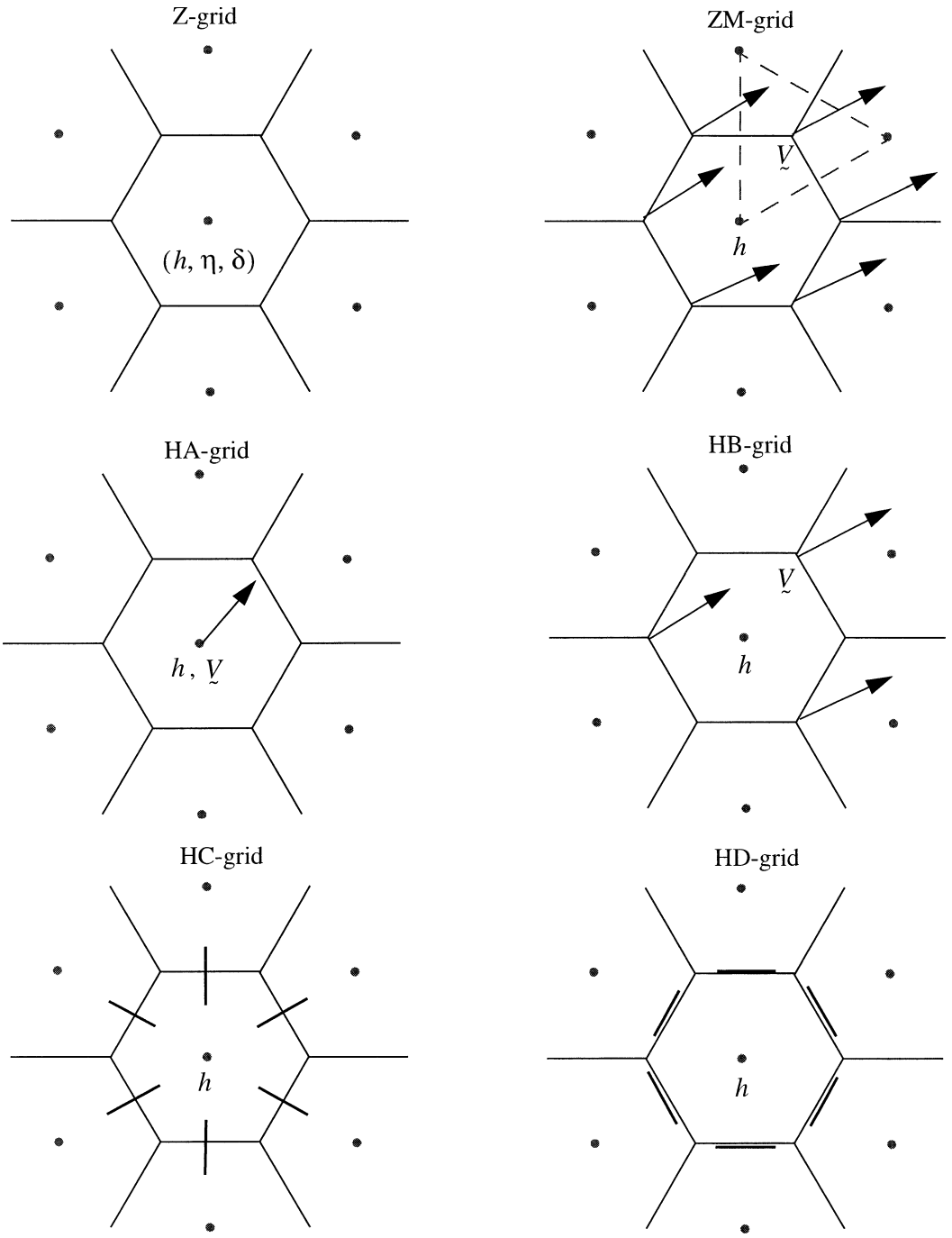

FIG. 1. The Z grid places mass, vorticity, and divergence at the center of each hexagon. The ZM grid places all scalars, such as mass, at the center of each hexagon and places all vectors, such as velocity, at every corner. Other possible grid staggerings, the HA, HB, HC, and HD grids, are discussed in the introduction and in Messinger (2000).

tionary geostrophic modes and asymmetric gravity wave propagation. While the severity of these problems is not yet fully known, it appears that the HB and HC grids are not optimal grid staggerings for the hexagonal grid system (Purser 1998). In this paper we will focus on the Z- and ZM-grid staggerings.

In RR, the ZM grid and Z grid were found to be consistent in the sense that when the discrete divergence and curl operators are applied to the discrete momentum equation, the Z-grid vorticity-divergence equations result. As discussed by RR, on a grid of hexagons the ZM grid has twice as many momentum points as mass points. This immediately implies that the velocity field is resolved on a finer mesh than the mass field. The

ramifications of resolving the prognostic variables at different resolutions are unclear. Ringler and Randall (2002) showed that the Z grid and ZM grid are equivalent in terms of their ability to conserve fundamental quantities such as mass, potential enstrophy, and total energy. The purpose of this paper is to explore more fully the relationship between the ZM grid and the Z grid, to determine if the ZM grid is, in fact, an attractive alternative to the Z grid.

This work is largely an extension of RR and for brevity we refer to that work frequently. In section 2 we provide a brief summary of the governing equations and highlight the consistency between the Z grid and the ZM grid. In section 3 we analyze the physical modes of the Z grid and ZM grid, and in section 4 we analyze the effect of resolving the velocity field at a higher level than the mass field in the ZM-grid system. The two grid-staggering systems are compared and contrasted in section 5. Also in section 5, we compare the ZM grid to another grid-staggering system proposed by Adcroft et al. (1999) that makes use of extra momentum points.

2. The equations, variables, and grids

a. The continuous equations

The nonlinear shallow-water equations have the form

$$\frac{\partial}{\partial t}\mathbf{V} = -(f + \zeta)\mathbf{k} \times \mathbf{V} - \nabla[K + g(h + h_s)], \quad (1)$$

$$\frac{\partial h}{\partial t} = -\nabla \cdot (h\mathbf{V}). \quad (2)$$

Here $\mathbf{V}$ is the horizontal velocity vector, ζ is the relative vorticity, f is the Coriolis parameter, g is the gravitational constant, K is the kinetic energy, h is the fluid depth, and h_s is the surface topography. Alternatively, we can take the curl and divergence of (1) to generate equations for the vorticity and divergence:

$$\frac{\partial \eta}{\partial t} = -\nabla \cdot (\eta\mathbf{V}), \quad (3)$$

$$\frac{\partial \delta}{\partial t} = \mathbf{k} \cdot \nabla \times (\eta\mathbf{V}) - \nabla^2[K + g(h + h_s)]. \quad (4)$$

Here $\eta \equiv f + \zeta$ and $\delta \equiv \nabla \cdot \mathbf{V}$ is the divergence. The vector momentum formulation and the vorticity-divergence formulation are equivalent given the appropriate boundary conditions.

b. The grid and discrete equations

We will discretize the shallow-water equations on a grid composed of perfect hexagons. The distance between grid-cell centers is d and the area of each cell is A_i.

By analogy to the continuous momentum formulation shown in (1) and (2), we express the discrete form of the shallow-water equations as follows:

$$\frac{\partial \mathbf{V}_c}{\partial t} = -\overline{\eta}_c \mathbf{k} \times \mathbf{V}_c - (\nabla K)_c - [\nabla g(h + h_s)]_c, \quad (5)$$

$$\frac{\partial h_i}{\partial t} + (\nabla \cdot \overline{h}\mathbf{V})_i = 0. \quad (6)$$

The momentum equation is defined at every grid-cell corner, while the mass equation is defined at every grid-cell center; this is the ZM grid introduced by RR. The subscript c denotes quantities defined at the cell corners, while the subscript i denotes quantities defined at the grid-cell centers. An overbar denotes quantities that are averaged from cell centers to the cell corners. The discrete gradient and divergence operators are both defined in RR.

If we apply the discrete divergence operator [RR, Eq. (2)] and curl operator [RR, Eq. (6)] to (5), we can convert the vector momentum formation to the scalar vorticity-divergence formulation:

$$\frac{\partial \eta_i}{\partial t} = -[\nabla \cdot (\overline{\eta}\mathbf{V}_c)]_i, \quad (7)$$

$$\frac{\partial \delta_i}{\partial t} = [\mathbf{k} \cdot \nabla \times (\overline{\eta}\mathbf{V}_c)]_i - \{\nabla^2[K + g(h + h_s)]\}_i. \quad (8)$$

The discrete form of the scalar formulation bears a striking resemblance to the continuous form [Eqs. (3) and (4)]. This is true because the actions of the discrete gradient, divergence, and curl operators are faithful to their respective continuous analogs. In particular, the vector identity $\nabla \times \nabla K = 0$ holds in the discrete case. The prognostic variables vorticity, divergence, and mass are all defined at the grid-cell centers; this is the Z grid introduced by Randall (1994).

When moving from the vector formulation to the scalar formulation, the Laplacian operator appears. The Laplacian operating on a scalar field is defined as

$$L(K) = \nabla \cdot \nabla K \quad (9)$$

in both the continuous system and the discrete system. We are not free to choose the discrete form of the Laplacian operator because it is defined by the gradient and divergence operators. With the gradient and divergence operators defined in RR, the Laplacian operator has the form

$$[L(K)]_0 = \frac{1}{\sqrt{3}A_0}(K_1 + K_2 + K_3 + K_4 + K_5 + K_6 - 6K_0), \quad (10)$$

where K_1 through K_6 are the immediate neighbors of K_0. The corresponding stencil is shown in Fig. 2.

3. Physical modes of the linearized shallow-water equations

a. The linearized equations

If we linearize (1) and (2) about a state of rest, we obtain

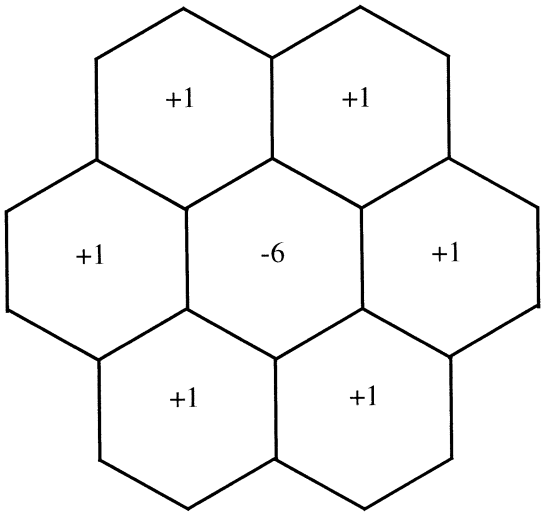

FIG. 2. Stencil for the second-order-accurate Laplacian operator on the hexagonal grid.

$$\frac{\partial}{\partial t}\mathbf{V} + f\mathbf{k} \times \mathbf{V} + g\nabla h = 0, \tag{11}$$

$$\frac{\partial h}{\partial t} + H\nabla \cdot \mathbf{V} = 0, \tag{12}$$

where H is the mean fluid depth. The corresponding linearized vorticity-divergence system of equations has the form

$$\frac{\partial \delta}{\partial t} - f\zeta + g\nabla^2 h = 0, \tag{13}$$

$$\frac{\partial \zeta}{\partial t} + f\delta = 0, \tag{14}$$

$$\frac{\partial h}{\partial t} + H\delta = 0. \tag{15}$$

b. The continuous case

If we assume wave solutions to the continuous system described by (13), (14), and (15), we obtain the familiar result

$$\left(\frac{\omega}{f}\right)^2 = 1 + \lambda^2(k^2 + l^2), \tag{16}$$

where $\lambda = (\sqrt{gH})/f$. Equation (16) accounts for the two inertia–gravity modes; the geostrophic solution, $\omega = 0$, is the third mode.

c. The discrete case

The linearized discrete vorticity-divergence system of equations is identical in form to (13), (14), and (15), except we use (10) as the discrete approximation of the Laplacian. We look for wave solutions of the form

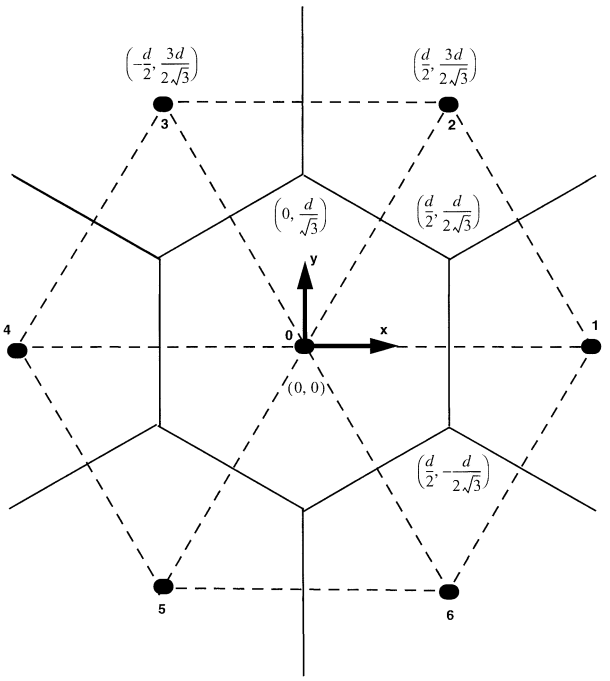

FIG. 3. A Cartesian coordinate system is centered on grid cell 0. The variable d is the distance between grid-cell centers.

$$h = \hat{h}e^{i\omega t}e^{i(kx_p + ly_q)}, \tag{17}$$

$$\delta = \hat{\delta}e^{i\omega t}e^{i(kx_p + ly_q)}, \tag{18}$$

$$\zeta = \hat{\zeta}e^{i\omega t}e^{i(kx_p + ly_q)}, \tag{19}$$

to the discrete analogs of (13), (14), and (15); this is the Z-grid system. In the discrete system, x_p and y_q can take only certain values. Referring to Fig. 3, we can write

$$x_p = pd, \tag{20}$$

$$y_q = \frac{qd}{\sqrt{3}}. \tag{21}$$

Integer and half-integer values of p and q are sufficient to specify the locations of all cell centers and all cell corners.

If we substitute (17), (18), and (19) into the discrete analogs of (13), (14), and (15), we find that

$$\left(\frac{\omega}{f}\right)^2 = 1 + \frac{8}{3}\left(\frac{\lambda}{d}\right)^2\left[\sin^2\left(\frac{kd}{2}\right) + \sin^2\left(\frac{kd}{4} + \frac{\sqrt{3}ld}{4}\right) + \sin^2\left(-\frac{kd}{4} + \frac{\sqrt{3}ld}{4}\right)\right]. \tag{22}$$

See appendix A for the details. Equation (22) accounts for the two inertia–gravity modes. The geostrophic mode, $\omega = 0$, is also a solution of the discrete system, and has already been factored out above. The Z grid

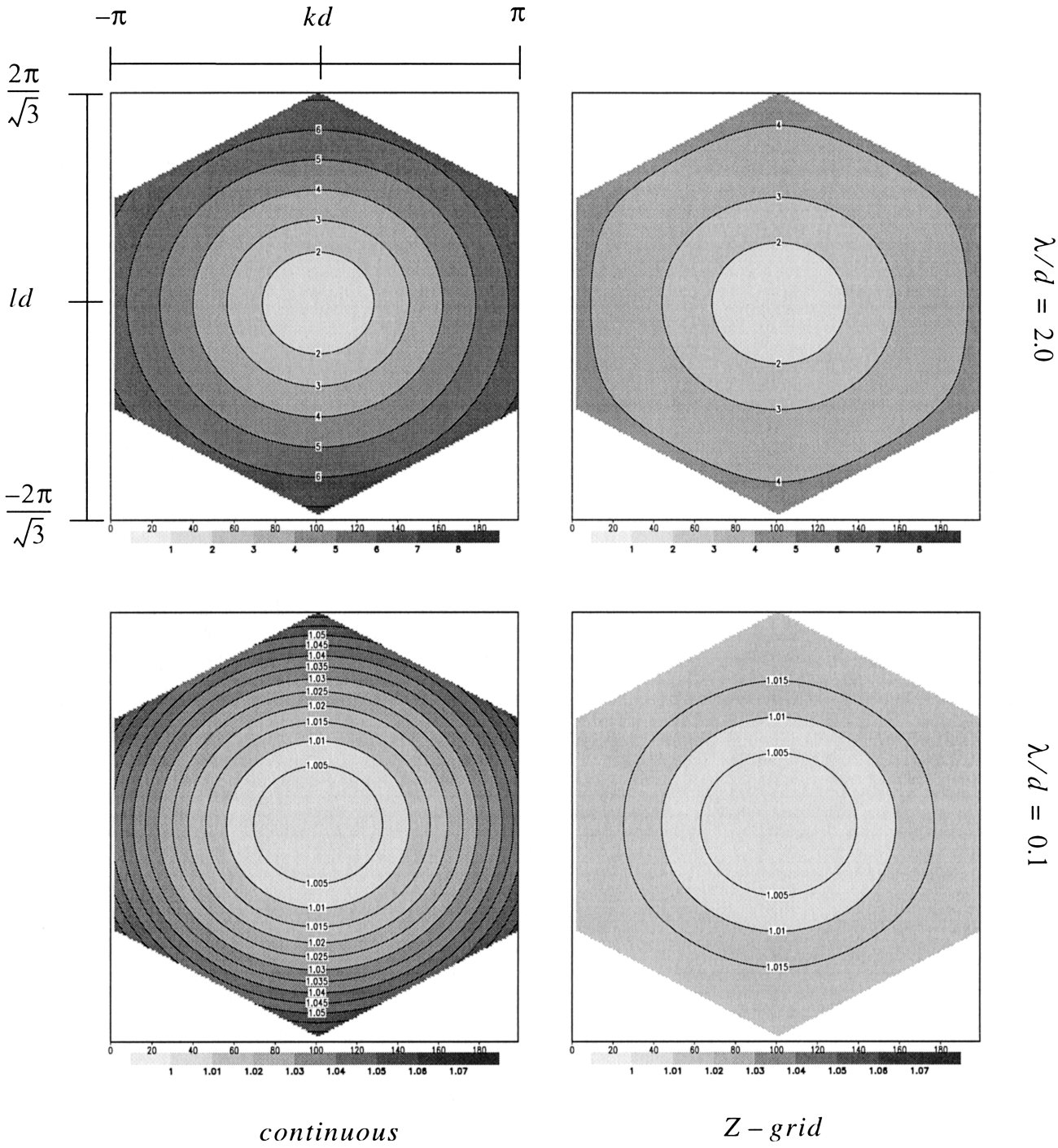

FIG. 4. The dispersion relation for values of (top) $\lambda/d = 2.0$ and (bottom) $\lambda/d = 0.1$. Both (left) the continuous solution and (right) the Z-grid solution are shown.

permits only the three physical modes; no computational modes exist. A plot of ω/f is shown in Fig. 4 for two values of λ/d: $\lambda/d = 2.0$ and $\lambda/d = 0.1$.

The nondimensional wavenumbers kd and ld can take on only certain discrete values. The collection of waves that exist on the hexagonal grid form a basis that can be used to completely describe the discrete grid data. The discrete modes that can exist on the square quadrilateral grid can be identified by solving the eigenvalue problem $\nabla^2 f = \lambda f$ with the appropriate boundary conditions. We solve this same eigenvalue problem, but on a hexagonal grid, in appendix B. The admissible values

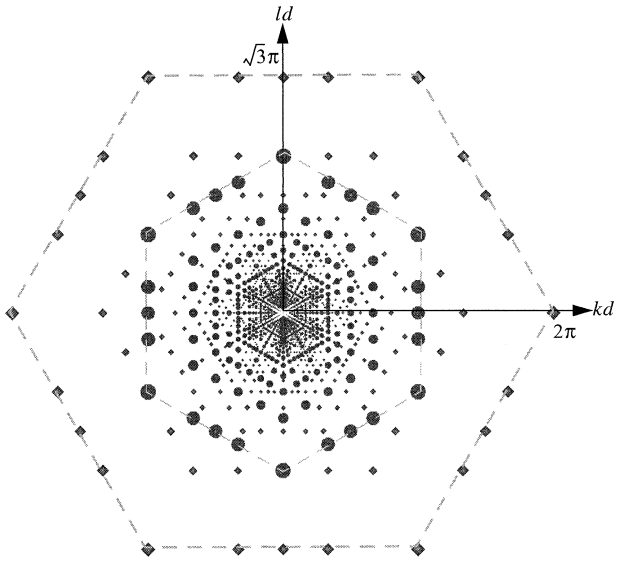

FIG. 5. The circles depict the wavenumbers that can exist on the Z grid. The diamonds depict the wavenumbers that can exist on the ZM grid. The inner hexagon that defines the region of the (*kd*, *ld*) plane spanned by the Z-grid modes will be called the Z space. Similarly, the outer hexagon will be called the ZM space. The region between these two spaces will be called the supplemental ZM space. See appendix B for details on how these modes were obtained.

of *kd* and *ld* for the Z grid are shown in Fig. 5 as circles. As is always the case, modes that are farther away from the origin are more thinly spaced than modes that are closer to the origin. The portion of the (*kd*, *ld*) plane spanned by the Z grid modes takes the shape of a hexagon. We refer to the inner hexagon shown in Fig. 5 as the Z space. In Fig. 4 we have plotted the discrete dispersion as a continuous function within the Z space. Furthermore, we have truncated the continuous solution to this same region to facilitate the comparison.

Recall that the group velocity is equal to the gradient of the frequency with respect to the wave vector. The energy associated with a wave packet is carried through the system at the group velocity. The continuous system has the property that energy projected onto any gravity wave mode will be carried away from the initial disturbance; that is, the group velocity is nonzero for all wavenumbers. We can infer the group velocity from Fig. 4. The slope of the dispersion relation plotted in Fig. 4 is proportional to the group velocity. Consistent with the results of Randall (1994), the dispersion relation on the Z grid is monotonically increasing with wavenumber and, therefore, the group velocity is positive definite for all wavenumbers.

The three physical modes of the Z-grid system are also solutions to the ZM-grid system. From a mathematical perspective, Eqs. (7) and (8) are simply linear combinations of (5), albeit very special linear combinations. Basic linear algebra allows us to conclude that the three solutions of the Z-grid system are also solutions of the ZM-grid system.

4. Ramifications of overresolving the velocity in the ZM-grid system

a. Determining the ZM-grid wavenumber space

Since the Z system has an unstaggered grid for mass, vorticity, and divergence, the resolved wavenumber space is identical for all three prognostic variables. This wavenumber space is the Z space and is shown by the inner hexagon in Fig. 5.

The ZM system's velocity equation populates a larger wavenumber space. This region is depicted by the outer hexagon in Fig. 5 and is referred to as the ZM space (See appendix B for details). The region of wavenumber space between the Z space and the ZM space will be referred to as the supplemental ZM space.

For clarity, it is useful to write down the ZM-grid equations for each of these wavenumber spaces. In the Z space, the full nonlinear equations are exactly what we would expect:

$$\frac{\partial \mathbf{V}_c}{\partial t} = -\overline{\eta}_c \mathbf{k} \times \mathbf{V}_c - (\boldsymbol{\nabla} K)_c - [\boldsymbol{\nabla} g(h + h_s)]_c, \tag{23}$$

$$\frac{\partial h_i}{\partial t} + (\boldsymbol{\nabla} \cdot \overline{h}\mathbf{V})_i = 0. \tag{24}$$

This is simply (5) and (6) repeated here for clarity. Within the supplemental ZM space, the equation set is dramatically different:

$$\frac{\partial \mathbf{V}_c}{\partial t} = -\overline{\eta}_c \mathbf{k} \times \mathbf{V}_c. \tag{25}$$

This can be understood as follows: First, within the supplemental ZM space there is no mass equation. Second, the gradient terms that normally occur on the rhs of the momentum equation are identically zero in this part of the wavenumber space. The reason for this is as follows: The gradient operator is a *linear* operator. If we set $g = L(f)$ where L is a linear operator, then we are guaranteed that the wavenumbers that exist in g are a subset of those that exist in f; that is, linear operators do not create new wavenumbers. Since the spectra of h, h_s, and K are zero in the supplemental ZM space, the gradient operator will be zero within the supplemental ZM space. So within the supplemental ZM space we are left with a ''momentum equation'' that includes only inertial oscillations.

Conceptually, we can think of the ZM system as being composed of two wavenumber spaces: the Z space plus the supplemental ZM space. Within the Z space, the dynamics of the ZM-grid system are identical to those of the Z-grid system. Within the supplemental ZM space, we are left with a highly simplified system that is not very similar of the continuous system.

It is important to note that only way energy can enter the supplemental ZM space is through the nonlinear terms on the rhs of (23). This implies that within the

context of the linearized shallow-water equations, the ZM system and Z system are identical. We have confirmed this finding by integrating the linearized shallow-water equations using the ZM system. If we use the same initial conditions, the ZM-grid solution tracks the Z-grid solution to within roundoff error.

Once energy is projected into the modes that reside in the supplemental ZM space, two things can happen. First, for those modes that have nonzero relative vorticity, some of the energy is projected back onto other modes via the inertial term on the rhs of (25). Second, for those modes that have zero relative vorticity, the energy simply accumulates. In the model, the relative vorticity of a velocity mode depends on the definition of the curl operator. For the curl operator defined in RR [their Eq. (6)], all of the velocity modes shown in Fig. 5 have nonzero relative vorticity, with the exception of the six modes that form the corners of the outer hexagon in Fig. 5. The easiest way to understand why these six modes have zero relative vorticity is as follows: The curl operator, like the gradient operator, is nonzero only in the Z space. During the application of the curl operator, all modes that reside in the supplemental ZM space will be aliased (or folded) back into the Z space. The six velocity modes that form the corners of the outer hexagon are aliased to the origin ($k = 0$ and $l = 0$). These modes disappear after the application of the curl operator. Since energy can accumulate only in these six modes, we interpret them as computational modes and we want to find a technique to limit the amount of energy that resides in these modes.

b. *Controlling the computational modes in the velocity field*

The first technique we use to limit the amount of energy in the supplemental ZM space can be called a filtering method. Given a velocity field containing energy in the supplemental ZM space, we first diagnose the vorticity and divergence fields. We then invert the elliptic equations to determine the streamfunction and velocity potential. [See RR Eqs. (10)–(14) for more details.] By differentiating these, we obtain a new velocity field that is the same as the original velocity field minus the energy contained in the supplemental ZM space. Recall that the scalar fields and gradient operator have zero amplitude in the supplemental ZM space. This filtering technique is equivalent to prognosing vorticity and divergence as opposed to the velocity; the filter is the Z-grid discretization.

The second technique is a dissipation method based on the discretization of the Laplacian of the velocity vector. Some form of viscous dissipation is required to control the downscale cascade of enstrophy and/or energy. In the two-dimensional shallow-water equations, dissipation of small-scale enstrophy is required to allow the upscale cascade of energy. Once formulated, the Laplacian operator is equally applicable to three-dimensional and two-dimensional simulations. The form of the dissipation operator used in RR is outlined in appendix C. This operator produces nonzero results only in the Z-space region shown in Fig. 5. It is therefore unable to dissipate the computational modes in the ZM space. An alternative formulation that is nonzero in both the Z space and ZM space is also outlined in appendix C.

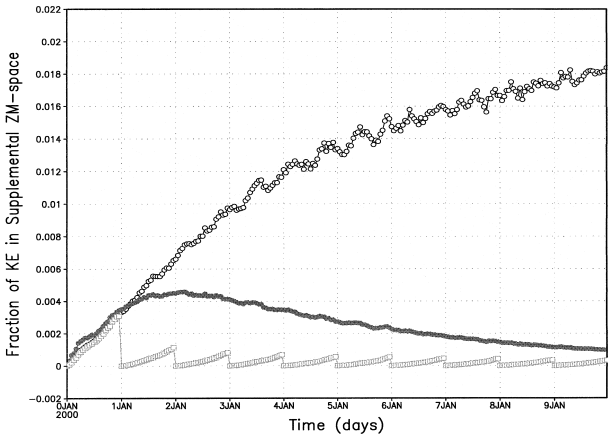

FIG. 6. The fractional amount of kinetic energy contained in the supplemental ZM space as a function of time for a simulation of 2D turbulence. Three simulations are shown: control (open circles), elliptic filtering once per day (squares), and viscous dissipation (closed circles).

In order to test these two techniques, we reran the 2D turbulence simulation described in RR. This simulation uses a doubly periodic f plane and ''white-noise'' initial conditions on vorticity, divergence, and fluid depth. These simulations require some type of small-scale dissipation in order to allow the upscale cascade of energy. The control simulation uses the same ∇^6 operator as used in RR (as outlined in appendix C). The elliptic filtering experiment uses this ∇^6 operator and, in addition, truncates the smallest velocity scales by the ''filtering'' method outlined above. The dissipation experiment uses an alternative formulation of the ∇^6 operator (as outlined in appendix C). We integrated each simulation for 10 simulated days. After each time step we determined the amount of kinetic energy contained in the supplemental ZM space. Figure 6 shows results from three simulations. The top curve is the amount of energy contained in the supplemental ZM space from the control simulation. After 10 days, 2% of the total kinetic energy in contained in this part of the wavenumber space. As is apparent from the figure, this curve is leveling off and asymptotes to a value of about 2.7% after about 100 days. The second curve shows what happens when we replace the velocity field with the filtered velocity field once per day. We find that after 10 simulated days less than 0.05% of the total kinetic energy is contained in the supplemental ZM space. The third curve shows what happens if we use an alternative formulation of the dissipation operator. After 10 days we find that less than 0.10% of the kinetic energy resides

in the supplemental ZM space. Both the filtering technique and the dissipation technique are able to limit the amount of energy that accumulates in the supplemental ZM space. Furthermore, both of these methods still yield appropriate energy and enstrophy spectras discussed in RR (not shown).

We have also performed several ''dirac-delta forcing experiments'' in another attempt to force these computational modes. In these experiments the fluid is in geostrophic balance at $t \leq 0$ and the system is inviscid in the sense that we do not impose any explicit dissipation. At $t = 0$ we impose a single-point momentum forcing of magnitude 1.0 m s^{-1} day^{-1} in the x direction. This forcing is held constant during the integration. This is equivalent to imposing a dirac-delta forcing to the momentum equation. Since the transform of the dirac-delta forcing is white, the forcing will project onto all the velocity modes shown in Fig. 5. Similar to the 2D turbulence experiments above, we diagnostically determine the amount of energy contained in the supplemental ZM space. For either the basic-state fluid at rest or flow in the x direction, we find that $\sim$0.5% of the kinetic energy is contained in the supplemental ZM space after 25 days of integration. We also performed these same experiments using the Z-grid formulation and find that the ZM solution and the Z solution are compatible.

5. Discussion and conclusions

We have analyzed the shallow-water equations on a hexagonal grid using both the vorticity-divergence formulation and the momentum formulation. When using the discrete vorticity-divergence form of the equations, we use the unstaggered Z grid (Randall 1994). When using the discrete momentum form of the equations, we use the ZM grid in which scalars are defined at grid-cell centers and vectors are defined at all grid-cell corners. As opposed to other staggering systems on the hexagonal grid (e.g., Mesinger 2000), we find that the Z and ZM grids both exhibit a monotonic increase in wave phase speed with increasing total wavenumber (Fig. 4), so that all waves have nonzero group velocities. Furthermore, the problems identified by Nickovic and Mesinger (discussed in Purser 1998) regarding nonstationary geostrophic modes and asymmetric gravity wave propagation on the HB and HC grids are not present on the Z grid or the ZM grid. The Z grid and ZM grid do not show these problems for two reasons. First, the Z and ZM grids each fully exploit the isotropy of the hexagonal grid. Second, the Z and ZM grids require no spatial averaging of variables during the course of integrating the linearized shallow-water equations.

The ZM grid has twice as many velocity points as mass points. As a result, the velocity field resolves a larger wavenumber space than the mass field (Fig. 5). The portion of the wavenumber space resolved by the Z grid was referred to as the Z space. The portion of the wavenumber space resolved by the ZM grid but not resolved by the Z grid is referred to as the supplemental ZM space in Fig. 5. The discrete dynamics in the ZM space are severely truncated and are not particularly representative of the continuous shallow-water equations.

In a simulation of 2D turbulence on an f plane, we showed that the amount of kinetic energy that accumulates in the supplemental ZM space remains small. After 10 days, only 2.0% of the fluid's kinetic energy was contained in the supplemental ZM space (Fig. 6). After 100 days, this value asymptotes to 2.7%. Furthermore, we demonstrated that there are at least two viable techniques to limit even this small amount of energy from existing in the supplemental ZM space. First, we showed that by inverting the divergence and vorticity to obtain the velocity potential and streamfunction, respectively, we could obtain a new velocity field that contained no energy in the supplemental ZM space. Second, we demonstrated that an alternative formulation of the dissipation operator was also able to limit the amount of energy in the supplemental ZM space.

The use of extra momentum points in order to improve the simulation of the physical modes of geostrophic adjustment is not unprecedented. Adcroft et al. (1999) combine the C-grid and D-grid staggerings on a quadrilateral grid to produce a simulation of the geostrophic adjustment process similar to the Z grid. The redundant momentum points result in computational modes. Adcroft et al. (1999) find that the computational modes take the form of inertial oscillations, and propose a time differencing scheme to damp these modes.

There are important differences, however, between the method outlined in Adcroft et al. (1999) and the ZM grid. First, while we have generalized the ZM-grid staggering to other geometries (to be discussed elsewhere), we have focused here on the hexagonal grid. Adcroft et al. (1999) focus on the quadrilateral grid. In addition to using different grid geometries, the two methods place the wind vectors at different locations. Adcroft et al. (1999) places wind vectors at the midpoints of grid-cell walls, whereas the ZM grid places wind vectors at the grid-cell corners. And finally, the scheme outlined by Adcroft et al. (1999) absolutely requires some methodology to limit the growth of the computational modes. While the ZM grid certainly requires continued vigorous testing, to date we have found no influence due to overresolving the velocity field on the stability of the simulation.

Overall, our findings lead us to conclude that both the Z- and ZM-grid staggerings on the hexagonal grid are excellent choices for finite-difference models. The Z-grid discretization does an exceptional job of modeling the physical modes. The ZM grid does an equally good job of simulating the physical modes. The ZM-grid system includes a supplemental wavenumber space due to its use of twice as many velocity points as mass

points. The obvious advantage of the ZM grid over the Z grid is computational efficiency. Since the ZM-grid system prognoses velocity instead of vorticity and divergence, the elliptic equations required with the Z-grid system are not required. In atmospheric modeling, for which the horizontal domain is both singly connected and periodic, Heikes and Randall (1995a,b) have implemented multigrid techniques that largely mitigate the computational burden imposed by these elliptic equations. We would still expect some computational advantage of the ZM grid over the Z grid in atmospheric modeling, particularly in models implemented on massively parallel machines (order 500 nodes or more) where multigrid techniques tend to scale poorly.

In the context of ocean modeling, the arguments for the ZM grid over the Z grid are more compelling. The implementation of the Z-grid elliptic equations in multiply connected ocean basins is complicated and, likely, computationally expensive. It would seem that the ZM grid is particularly well suited for ocean general circulation modeling.

Acknowledgments. We would like to thank Ross Heikes and Alistair Adcroft for useful discussions and comments on an earlier draft. We would also like to thank Akio Arakawa for his comments and for suggesting the ''dirac-delta function'' forcing experiments. This work was supported by the U.S. Department of Energy's Climate Change Prediction Program under Grant DE-FG03-98ER62611 to Colorado State University.

APPENDIX A

Linear Modes of the Z-Grid Model

The discrete transformed equations have the form

$$\omega\hat{\delta} + if\hat{\zeta} + ig\hat{L}\hat{h} = 0, \tag{A1}$$

$$-if\hat{\delta} + \omega\hat{\zeta} + 0 = 0, \tag{A2}$$

$$-iH\hat{\delta} + 0 + \omega\hat{h} = 0. \tag{A3}$$

Here the $\hat{}$ symbol represents the transformed variable and $\hat{L}$ is the transform of the discrete Laplacian shown in (10). If we set the determinant of this system to zero, we obtain the formal dispersion relation of

$$\left(\frac{\omega}{f}\right)^2 = 1 - gH\hat{L}. \tag{A4}$$

As described in Randall (1994), on the Z grid the discrete dispersion relation is completely determined by the discrete Laplacian. Referring to Fig. 3, we can rewrite (10) as

$$L(h) = \frac{1}{\sqrt{3}A_0}[(h_1 - h_0) - (h_0 - h_4) + (h_2 - h_0) - (h_0 - h_5) + (h_3 - h_0) - (h_0 - h_6)]. \tag{A5}$$

We find $\hat{L}$ by substituting (17) into the rhs of (A5). Focusing on the first term on the rhs of (A5) we find

$$(h_1 - h_0) = \hat{h}(e^{ikd} - e^0) = 2i\hat{h}e^{ikd/2}\sin\left(\frac{kd}{2}\right). \tag{A6}$$

Similarly, the transform of second term of the rhs of (A5) is

$$-(h_0 - h_4) = -\hat{h}(e^0 - e^{-ikd}) = -2i\hat{h}e^{-ikd/2}\sin\left(\frac{kd}{2}\right). \tag{A7}$$

Equations (A6) and (A7) can be combined as

$$2i\hat{h}e^{ikd/2}\sin\left(\frac{kd}{2}\right) - 2i\hat{h}e^{-ikd/2}\sin\left(\frac{kd}{2}\right) = -4\hat{h}\sin^2\left(\frac{kd}{2}\right). \tag{A8}$$

The transform of the third and fourth terms on the rhs of (A5) reduces to

$$(h_2 - h_0) - (h_0 - h_5) = -4\hat{h}\sin^2\left(\frac{kd}{4} + \frac{\sqrt{3}ld}{4}\right), \tag{A9}$$

and, similarly, the last two terms on the rhs of (A5) reduce to

$$(h_3 - h_0) - (h_0 - h_6) = -4\hat{h}\sin^2\left(\frac{-kd}{4} + \frac{\sqrt{3}ld}{4}\right). \tag{A10}$$

We can then write $\hat{L}$ as

$$\hat{L} = \frac{-8}{3d^2}\left[\sin^2\left(\frac{kd}{2}\right) + \sin^2\left(\frac{kd}{4} + \frac{\sqrt{3}ld}{4}\right) + \sin^2\left(-\frac{kd}{4} + \frac{\sqrt{3}ld}{4}\right)\right], \tag{A11}$$

where we have used the relation of $A_0 = \sqrt{3}d/2$. Substituting (A11) into (A4) yields (22).

APPENDIX B

Modes of the Hexagonal Grid

We solve the eigenvalue problem

$$\nabla^2 f = \lambda f, \tag{B1}$$

where f is a scalar function, to determine the set of modes that can exist on the hexagonal grid. We chose this eigenvalue problem for several reasons. First, since the Laplacian operator is self-adjoint, we are guaranteed that the eigenvalues will be real and that the eigenvectors will be orthogonal and will form a complete basis

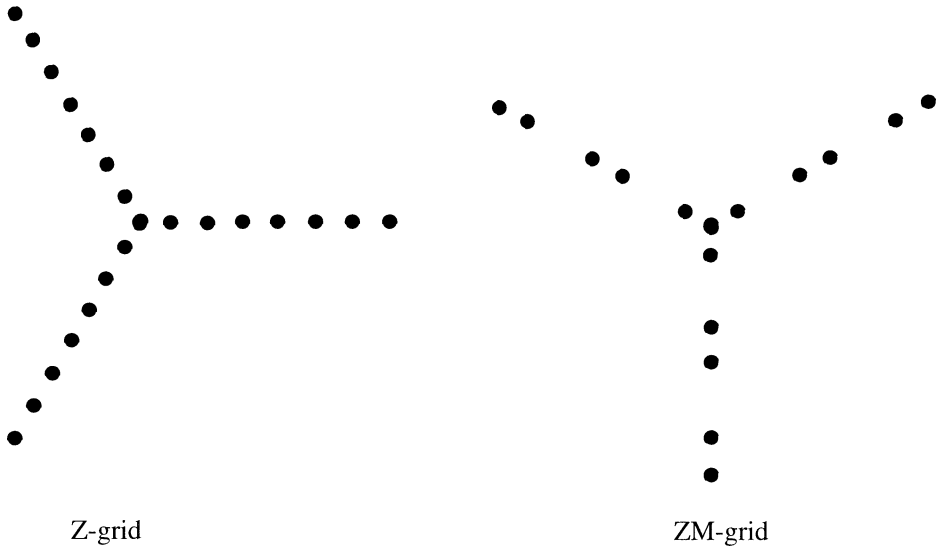

FIG. B1. The grid points for the Z grid and the ZM grid. The Z grid is symmetric with respect to rotations of 60°. The ZM grid is symmetric with respect to rotations of 120°. The grid points along directions of symmetry are shown.

(Greenberg 1978). This means that if we describe f in terms of these eigenvectors, we will have a complete description of f. Second, (B1) is ubiquitous in the modeling of vibrational and wave phenomena. By assuming wavelike solutions to (B1), we find that the eigenvectors have the structures of waves. On the plane, (B1) can be used as a means of determining discrete Fourier modes. On the sphere, the counterpart of (B1) is used to find the spherical harmonics.

The discrete analog to (B1) is

$$\nabla^2 f_{(p,q)} = \lambda f_{(p,q)}, \tag{B2}$$

where (p, q) describes the location of a grid point as described in (20) and (21). If we assume wavelike solutions for $f_{(p,q)}$ of the form

$$f = \hat{f} e^{i(kx_p + ly_q)} \tag{B3}$$

in a fashion similar to (17), we find that (B2) reduces to

$$\frac{-8}{3d^2}\left[\sin^2\left(\frac{kd}{2}\right) + \sin^2\left(\frac{kd}{4} + \frac{\sqrt{3}ld}{4}\right) + \sin^2\left(-\frac{kd}{4} + \frac{\sqrt{3}ld}{4}\right)\right] = \lambda. \tag{B4}$$

See appendix A for the details of how (B4) is derived. Note that the three waves in (B4) can be interpreted as wave vectors $((kd/2)\mathbf{e}_1$, $(kd/4)\mathbf{e}_1 + (\sqrt{3}ld/4)\mathbf{e}_2$, $(kd/4)\mathbf{e}_1 + (\sqrt{3}ld/4)\mathbf{e}_2)$. These waves point across cell walls; that is, the waves point along the directions of symmetry of the hexagonal grid. We call these three directions (α, β, γ), respectively.

Only discrete values of kd and ld are permitted on the hexagonal grid; our primary purpose within this appendix is to determine these values. These values are, of course, strongly influenced by the boundary conditions. Since our immediate application is the atmosphere, periodic boundary conditions in all directions are most appropriate. We therefore require solutions of (B4) to be periodic in the α, β, and γ directions.

Focusing on the first term on the lhs of (B4), we note that

$$\sin^2\left(\frac{kd}{2}\right) = \frac{1}{2}[1 - \cos(kd)]. \tag{B5}$$

The angular distance traveled by the wave between adjacent grid points is kd. In order for this wave to be periodic, we require

$$kd[(i + i_\alpha) - i] = \pm 2\pi \qquad (i_\alpha \geq 2). \tag{B6}$$

Stated in words, we require the angular distance traveled between grid point i and $i + i_\alpha$ to be $\pm 2\pi$. The variable i_α is an arbitrary integer. We require i_α to be greater than or equal to 2 since at least three independent grid points are required to resolve a wave. Simplifying (B6) and writing corresponding conditions on the other two terms in (B4), we obtain the following system of equations:

$$kd = \frac{\pm 2\pi}{i_\alpha} \qquad (i_\alpha \geq 2), \tag{B7}$$

$$\frac{kd}{2} + \frac{\sqrt{3}ld}{2} = \frac{\pm 2\pi}{i_\beta} \qquad (i_\beta \geq 2), \tag{B8}$$

$$-\frac{kd}{2} + \frac{\sqrt{3}ld}{2} = \frac{\pm 2\pi}{i_\gamma} \qquad (i_\gamma \geq 2). \tag{B9}$$

For a given kd and ld to be a possible solution of (B4), we require (B7), (B8), and (B9) to be satisfied. Equations (B7), (B8), and (B9) describe lines in the (kd, ld)

plane. The values of *kd* and *ld* that simultaneously satisfied by these three equations are shown as circles in Fig. 5.

In addition to finding the set of modes that can exist on the set of points defined by the centers of the hexagons (the Z grid), we also want to determine the set of modes that can exist on the set of points defined by the corners of the hexagons (the ZM grid). The grid points along the directions of symmetry that define the Z grid and ZM grid are shown in Fig. B1. We see that there are three differences between the two grid structures. First, the ZM grid is rotated 30° relative to the Z grid. Second, the ZM grid points are $1/\sqrt{3}$ closer than the Z grid points. And finally, every third grid point on the ZM grid is omitted. The distances between adjacent ZM grid points follow the sequence $\{\ldots\ldots, d/\sqrt{3}, 2d/\sqrt{3}, d/\sqrt{3}, 2d/\sqrt{3}, \ldots\ldots\}$; this corresponds to a uniform grid with every third grid point missing. Given these relationships between the Z grid and the ZM grid, we can infer the ZM-grid modes: these modes are rotated 30° relative to the Z grid and ''stretched'' by a factor of $\sqrt{3}$. These modes are shown as diamonds in Fig. 5.

Figure 5 also provides a nice interpretation of the ZM-grid computational modes. Recall that scalar data, such as relative vorticity, is defined on the Z grid, while velocity is defined on the ZM grid. So the circles in Fig. 5 define the vorticity modes (called the Z space), while the diamonds define the velocity modes (called the ZM space). Upon application of the curl (or divergence) operator, all of the velocity modes that lie outside the region defined by Z space will be aliased (or folded) back into the Z-space region. The six velocity modes that lie farthest away from the origin (these modes define the corners of the outer hexagon in Fig. 5) are folded back to the origin. These modes are aliased to the wavenumber $k = 0$ and $l = 0$ and are, thus, ''invisible'' to the vorticity field.

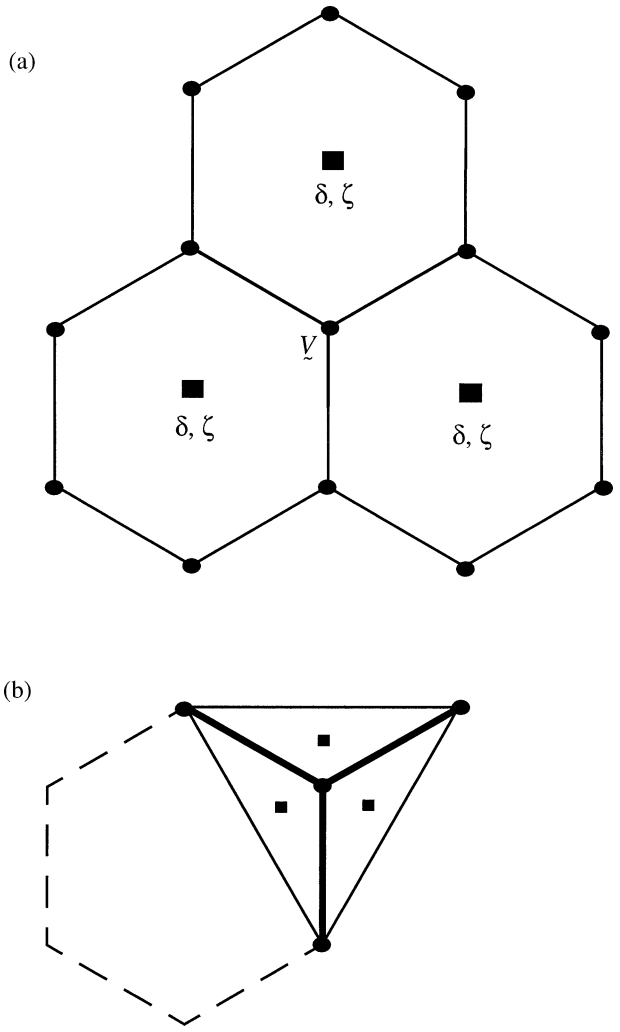

FIG. C1. This figure outlines two discretizations of the Laplacian of a vector. The vector velocity field is defined at the circles, while the divergence, δ, and vorticity, ζ, are defined at the squares. (a) Divergence and vorticity are computed by taking the line integral of **V** around each hexagon. (b) Divergence and vorticity are computed by integrating around each triangle. The Laplacian of *V* can then be approximated at the center velocity point by fitting a plane through the three divergence and vorticity data points.

APPENDIX C

Formulations of the Dissipation Operators

This appendix discusses two discretizations of the Laplacian of a vector. First, we outline the method used in RR. Second, we discuss an alternative formulation of the dissipation operator that acts to dissipate the smallest scales of motion present in the discrete velocity field. Both formulations use the vector identity

$$\nabla^2\mathbf{V} = \boldsymbol{\nabla}\delta + \boldsymbol{\nabla} \times \zeta \qquad \text{(C1)}$$

as the definition of the Laplacian of a vector. In RR, we chose the stencil shown in Fig. C1a to discretize (C1). The merit of this formulation is that it uses the same discrete operators that are used in the rest of the shallow-water model. The divergence, δ, and relative vorticity, ζ, are computed at the cell centers by applying the discrete divergence and curl operators shown in RR's Eqs. (2) and (6). The gradient of δ and ζ is the slope of the plane fit through the three data points. The one problem with this formulation is that it only resolves scales that exist inside the Z space shown in Fig. 5; the operator is identically zero in the supplemental ZM space. We construct higher-order operators, such as ∇^6, by recursive application of the ∇^2 operator. We use a coefficient of 1.0×10^{24} m^6 s^{-1} with this ∇^6 operator, which is used in the control simulation.

Alternatively, we can discretize (C1) on the smallest stencil possible in order to capture the smallest variations present on the grid. The stencil is shown in Fig. C1b. Given **V** at the cell corners, we compute δ and ζ for each triangle by computing the area-normalized line

integral of $\mathbf{V} \cdot \mathbf{r}$ and $\mathbf{V} \cdot \mathbf{t}$ around the perimeter of each triangle. This results in an approximation of δ and ζ at the squares shown in Fig. C1b. We then approximate the gradients of δ and ζ as the slopes of the planes fit through these three points. This dissipation operator has several merits worth noting. First, it uses the minimum number of points possible in order to approximate the Laplacian in two-space. As a result of using the minimum number of points, the discrete operators captures or ''sees'' the smallest scales resolved by the grid. We use a coefficient of 1.0×10^{20} m^6 s^{-1} for this formulation of the ∇^6 operator.

REFERENCES

Adcroft, A. J., C. N. Hill, and J. C. Marshall, 1999: A new treatment of the Coriolis terms in C-grid models a both high and low resolutions. *Mon. Wea. Rev.,* **127,** 1928–1936.

Arakawa, A., and V. R. Lamb, 1977: Computational design of the basic dynamical process of the UCLA general circulation model. *Methods in Computational Physics,* J. Chang, Ed., Vol. 17, Academic Press, 173–265.

Greenberg, M. D., 1978: *Foundations of Applied Mathematics.* Prentice Hall, 636 pp.

Heikes, R., and D. A. Randall, 1995a: Numerical integration of the shallow-water equations on a twisted icosahedral grid. Part I: Basic design and results of tests. *Mon. Wea. Rev.,* **123,** 1862–1880.

——, and ——, 1995b: Numerical integration of the shallow-water equations on a twisted icosahedral grid. Part II: A detailed description of the grid and an analysis of numerical accuracy. *Mon. Wea. Rev.,* **123,** 1881–1887.

Mesinger, F., 2000: Numerical Methods: The Arakawa approach, horizontal grid, global, and limited-area modeling. *General Circulation Model Development,* D. A. Randall, Ed., Academic Press, 373–419.

Purser, R. J., 1998: Non-standard grids. *Seminar on Recent Developments in Numerical Methods for Atmospheric Modelling,* Reading, United Kingdom, European Center for Medium-Range Weather Forecasts, 44–72.

Randall, D. A., 1994: Geostrophic adjustment and the finite-difference shallow-water equations. *Mon. Wea. Rev.,* **122,** 1371–1377.

Ringler, T. D., and D. A. Randall, 2002: A potential enstrophy and energy conserving numerical scheme for solution of the shallow-water equations on a geodesic grid. *Mon. Wea. Rev.,* **130,** 1397–1410.